

Study of $B_s \rightarrow (\eta, \eta', \phi) \ell \bar{\ell}$ Decays

C.Q. Geng and C.C. Liu

*Department of Physics, National Tsing Hua University
Hsinchu, Taiwan, Republic of China*

*Theory Group, TRIUMF
4004 Wesbrook Mall, Vancouver, B.C. V6T 2A3, Canada*

Abstract

We study the rare decays of $B_s \rightarrow M_s \ell \bar{\ell}$ ($M_s = \eta, \eta', \phi$ and $\ell = \nu, e, \mu, \tau$) in the standard model. With the hadronic form factors evaluated in the light front and constituent quark models, we estimate the decay branching ratios, respectively. We also discuss the longitudinal lepton polarization and forward-backward asymmetries.

1 Introduction

The inclusive flavor-changing neutral current (FCNC) process of $B \rightarrow X_s \ell^+ \ell^-$, which is suppressed and induced by electroweak penguin and box diagrams in the standard model (SM), has been recently observed by the Belle detector at the KEKB e^+e^- asymmetric-energy collider [1] with the branching ratio (BR) of $(6.1 \pm 1.4^{+1.3}_{-1.1}) \times 10^{-6}$ for di-lepton masses greater than 0.2 GeV , where ℓ is either an electron or a muon and X_s is a hadronic recoil system that contains a kaon. The exclusive decay of $B \rightarrow K \ell^+ \ell^-$ has been measured with the BR of $(0.75^{+0.25}_{-0.21} \pm 0.09) \times 10^{-6}$ [2] and $(0.78^{+0.24+0.11}_{-0.20-0.18}) \times 10^{-6}$ [3, 4] at the Belle and Babar detectors by using 29.1 fb^{-1} and 77.8 fb^{-1} data samples, which agree with the theoretically estimated values [5, 6, 7, 8], respectively. Experimental searches at the B-factories [2, 3, 4] for $B \rightarrow K^* \ell^+ \ell^-$ are also close to the theoretical predicted ranges [5, 6, 7, 8]. At Babar, an excess of events over background with estimated significance of 2.8σ has been observed and $BR(B \rightarrow K^* \ell^+ \ell^-) = (1.68^{+0.68}_{-0.58} \pm 0.28) \times 10^{-6}$ has been obtained [4]. It is clear that these FCNC rare decays are important for not only testing the SM but probing new physics.

In this paper, we study another type of the exclusive decays, $B_s \rightarrow M_s \ell^+ \ell^-$ ($M_s = \eta, \eta', \phi$), related to the transition of $b \rightarrow s \ell^+ \ell^-$ at the quark level as shown in Figure 1. The decays of $B_s \rightarrow \eta \ell^+ \ell^-$ have been estimated in Ref. [9] and $B_s \rightarrow \phi \ell^+ \ell^-$ have been explored in Refs. [10, 11]. Recently, the Collider Detector at Fermilab (CDF) Collaboration has given an upper limit of $BR(B_s \rightarrow \phi \mu^+ \mu^-) < 6.7 \times 10^{-5}$ at a 95% confidence level [12]. In future, more data on the B_s decays will be collected in various hadron colliders such as CDF-II, HERA-B and ATLAS. To study the decay rates and branching ratios, we need to calculate the transition form factors of the vector, axial-vector and tensor currents. There are many different candidates for this purpose, *e.g.*, lattice QCD [13], QCD sum rule [14], and relativistic quark models. In this work, we use the framework of the light front quark model (LFQM) [15, 16] to evaluate the form factors and compared with those in the constituent quark model (CQM) [17].

This paper is organized as follows. In Sec. 2, we calculate the form factors for $B_s \rightarrow \eta, \eta'$ and ϕ transitions in the LFQM. We also present the results with those in the CQM. In Sec. 3, we study the decay rates and asymmetries of $B_s \rightarrow P(V) \ell^+ \ell^-$ with $\ell = \nu, e, \mu, \tau$ and $P(V)$ = pseudoscalar (vector) mesons. Our conclusions are given in Sec. 4.

2 Form Factors

2.1 Effective Hamiltonians and Matrix Elements

The contributions to the decays of $B_s \rightarrow M_s \ell \bar{\ell}$ ($M_s = \eta, \eta', \phi$) in the SM arise from the W -box and $Z(\gamma)$ - penguin diagrams as seen in Figure 1. The effective Hamiltonians of $b \rightarrow s \nu \bar{\nu}$ and $b \rightarrow s \ell^+ \ell^-$ are given by [18]

$$\mathcal{H} = \frac{G_F}{\sqrt{2}} \frac{\alpha}{2\pi \sin^2 \theta_W} \lambda_t D(x_t) \bar{b} \gamma_\mu (1 - \gamma_5) s \bar{\nu} \gamma_\mu (1 - \gamma_5) \nu, \quad (1)$$

and

$$\mathcal{H} = \frac{G_F \alpha \lambda_t}{\sqrt{2} \pi} \left[C_8^{eff}(\mu) \bar{s}_L \gamma_\mu b_L \bar{\ell} \gamma^\mu \ell + C_9 \bar{s}_L \gamma_\mu b_L \bar{\ell} \gamma^\mu \gamma_5 \ell - \frac{2m_b C_7(\mu)}{q^2} \bar{s}_L i \sigma_{\mu\nu} q^\nu b_R \bar{\ell} \gamma^\mu \ell \right], \quad (2)$$

respectively, where $x_t \equiv m_t^2/m_W^2$, $\lambda_t = V_{ts}^* V_{tb}$, $D(x_t)$ is the top-quark loop function [19, 20] and $C_8(\mu)$, C_9 and $C_7(\mu)$ are Wilson coefficients (WCs) with their explicit expressions given in Ref. [20] for the SM. We note that C_9 is free of the μ scale. Besides the short-distance (SD) contributions, the main effect on the decays is from $c\bar{c}$ resonant states such as Ψ and Ψ' , *i.e.*, the long-distance (LD) contributions. To including the LD effect, in Eq. (2) we replace $C_8(\mu)$ by $C_8^{eff}(\mu)$ [8, 20], given by

$$C_8^{eff}(\mu) = C_8(\mu) + (3C_1(\mu) + C_2(\mu)) \left(h(x, s) + \frac{3}{\alpha} \sum_{j=\Psi, \Psi'} k_j \frac{\pi \Gamma(j \rightarrow l^+ l^-) M_j}{q^2 - M_j^2 + i M_j \Gamma_j} \right), \quad (3)$$

where we have neglected the small WCs, and $h(x, s)$ describes the one-loop matrix elements of operators $O_1 = \bar{s}_\alpha \gamma^\mu P_L b_\beta \bar{c}_\beta \gamma_\mu P_L c_\alpha$ and $O_2 = \bar{s} \gamma^\mu P_L b \bar{c} \gamma_\mu P_L c$ [20], M_j (Γ_j) are the masses (widths) of intermediate states, and $k_j = -1/(3C_1(\mu) + C_2(\mu))$ [8]. The WCs at the scale of $\mu \sim m_b \sim 4.8$ GeV are shown in Table 1.

Table 1: Wilson coefficients for $m_t = 170$ GeV and $\mu = 4.8$ GeV.

| WC | C_1 | C_2 | C_7 | C_8 | C_9 |
|----|--------|-------|--------|-------|--------|
| | -0.226 | 1.096 | -0.305 | 4.186 | -4.559 |

To get the transition matrix elements of $B_s \rightarrow M_s$ with various quark models, we parametrize them in terms of the relevant form factors as follows:

$$\begin{aligned} \langle \eta_s(p_2) | V_\mu | B_s(p_1) \rangle &= F_+(q^2) P_\mu + F_-(q^2) q_\mu, \\ \langle \eta_s(p_2) | T_{\mu\nu} q^\nu | B_s(p_1) \rangle &= \frac{1}{m_{B_s} + m_{\eta(\eta')}} \left[q^2 P_\mu - (P \cdot q) q_\mu \right] F_T(q^2), \end{aligned}$$

$$\begin{aligned}
\langle \phi(p_2, \epsilon) | V_\mu \mp A_\mu | B_s(p_1) \rangle &= \frac{1}{m_{B_s} + m_\phi} \left[-iV(q^2) \varepsilon_{\mu\nu\alpha\beta} \epsilon^{*\nu} P^\alpha q^\beta \right. \\
&\quad \left. \pm A_0(q^2) (P \cdot q) \epsilon_\mu^* \pm A_+(q^2) (\epsilon^* \cdot p_1) P_\mu \right. \\
&\quad \left. \pm A_-(q^2) (\epsilon^* \cdot p_1) q_\mu \right], \\
\langle \phi(p_2, \epsilon) | (T_{\mu\nu} \pm T_{\mu\nu}^5) q^\nu | B_s(p_1) \rangle &= -ig(q^2) \varepsilon_{\mu\nu\alpha\beta} \epsilon^{*\nu} P^\alpha q^\beta \\
&\quad \pm a_0(q^2) (P \cdot q) \left[\epsilon_\mu^* - \frac{1}{q^2} (\epsilon^* \cdot q) q_\mu \right] \\
&\quad \pm a_+(q^2) (\epsilon^* \cdot p_1) \left[P_\mu - \frac{1}{q^2} (P \cdot p_1) q_\mu \right], \quad (4)
\end{aligned}$$

where m_M ($M = B_s, \eta, \eta'$ and ϕ) are the meson masses, $p_1(p_2)$ is the momentum of the initial (final) meson, ϵ is the polarization vector of the vector meson ϕ , $P = p_1 + p_2$, $q = p_1 - p_2$, $V_\mu = \bar{q}_2 \gamma_\mu q_1$, $A_\mu = \bar{q}_2 \gamma_\mu \gamma_5 q_1$, $T_{\mu\nu} = \bar{q}_2 i \sigma_{\mu\nu} q_1$, $T_{\mu\nu}^5 = \bar{q}_2 i \sigma_{\mu\nu} \gamma_5 q_1$, and $F_{\pm,T}$, V , $A_{0,\pm}$, g , and $a_{0,\pm}$ are the form factors.

The daughter mesons in Eq. (4) are in the bound state $\bar{s}s$ with the physical masses, m_η , $m_{\eta'}$, and m_ϕ . In the transfer matrix elements of $B_s \rightarrow \eta_s$, there are two sets of the form factors, $F_{\pm,T}$, corresponding m_η and $m_{\eta'}$, respectively.

The pseudoscalar meson η and η' composed by the states $u\bar{u}$, $d\bar{d}$ and $s\bar{s}$ can be expressed as the mixtures of two orthogonal states η_q and η_s , given by $\eta_q = (u\bar{u} + d\bar{d})/\sqrt{2}$ and $\eta_s = s\bar{s}$ [21]. Explicitly, one has that

$$\begin{pmatrix} \eta \\ \eta' \end{pmatrix} = \begin{pmatrix} \cos \theta & -\sin \theta \\ \sin \theta & \cos \theta \end{pmatrix} \begin{pmatrix} \eta_q \\ \eta_s \end{pmatrix}, \quad (5)$$

with $\theta = (39.3^\circ \pm 1.0^\circ)$ [21]. To study the decay rates of $B_s \rightarrow (\eta, \eta') \ell \bar{\ell}$, we will first consider $B_s \rightarrow \eta_s(m_\eta) \ell \bar{\ell}$ and $B_s \rightarrow \eta_s(m_{\eta'}) \ell \bar{\ell}$ and then use

$$\begin{aligned}
\Gamma(B_s \rightarrow \eta \ell \bar{\ell}) &= \sin^2 \theta \Gamma[B_s \rightarrow \eta_s(m_\eta) \ell \bar{\ell}] \\
\Gamma(B_s \rightarrow \eta' \ell \bar{\ell}) &= \cos^2 \theta \Gamma[B_s \rightarrow \eta_s(m_{\eta'}) \ell \bar{\ell}]. \quad (6)
\end{aligned}$$

2.2 Light Front Quark Model

Since the calculations of the transition form factors in Eq. (4) belong to the nonperturbative regime, the phenomenological quark models may be needed. One thing worthwhile mentioning here is that all of form factors will be studied in the time-like physical meson decay region of $0 \leq q^2 \leq (m_{B_s} - m_{\eta, \eta', \phi})^2$. As q^2 decreases, corresponding to the increasing recoil momentum, we have to start considering relativistic effects seriously. In particular, at the maximum recoil point of $q^2 = 0$ where the final meson can be highly relativistic, there is no reason to expect that the non-relativistic quark model is still applicable. A

consistent treatment of the relativistic effects of the quark motion and spin in a bound state is a main issue of the relativistic quark model.

The LFQM [22, 23] is the relativistic quark model in which a consistent and fully relativistic treatment of quark spins and the center-of-mass motion can be carried out [24]. The LFQM has been applied to study the heavy-to-heavy and heavy-to-light weak decay form factors in the timelike region [15, 25]. These calculations are based on the observation [26] that in the frame where the momentum transfer is purely longitudinal, i.e., $q_\perp = 0$, $q^2 = q^+q^-$ covers the entire range of momentum transfers. The price one has to pay is that, besides the conventional valence-quark contribution, one must also consider the non-valence configuration (or the so-called Z graph) arising from the quark-pair creation in the vacuum. Unfortunately, a reliable way of estimating the Z graph is still lacking. However, the non-valence contribution vanishes if $q^+ = 0$, and it is supposed to be unimportant for heavy-to-heavy transitions [15]. In this paper, all of the values obtained from the LFQM are based on the formulas in Refs. [15, 16].

A meson bound state consisting of a heavy quark q_1 and an antiquark q_2 with total momentum P and spin S can be written as

$$|M(P, S, S_z)\rangle = \int \frac{dp_1^+ d^2 p_{1\perp}}{2(2\pi)^3} \frac{dp_2^+ d^2 p_{2\perp}}{2(2\pi)^3} 2(2\pi)^3 \delta^3(\tilde{P} - \tilde{p}_1 - \tilde{p}_2) \times \sum_{\lambda_1, \lambda_2} \Psi^{SS_z}(\tilde{p}_1, \tilde{p}_2, \lambda_1, \lambda_2) |q_1(p_1, \lambda_1) \bar{q}_2(p_2, \lambda_2)\rangle, \quad (7)$$

where p_1 and p_2 are the on-mass-shell light front momenta,

$$\tilde{p} = (p^+, p_\perp), \quad p_\perp = (p^1, p^2), \quad p^- = \frac{m^2 + p_\perp^2}{p^+}, \quad (8)$$

with

$$p_1^+ = (1-x)P^+, \quad p_2^+ = xP^+, \\ p_{1\perp} = (1-x)P_\perp + k_\perp, \quad p_{2\perp} = xP_\perp - k_\perp. \quad (9)$$

Here (x, k_\perp) are the light-front relative momentum variables, and \vec{k}_\perp is the component of the internal momentum $\vec{k} = (\vec{k}_\perp, k_z)$. The momentum-space wave-function Ψ^{SS_z} in Eq. (7) can be expressed as

$$\Psi^{SS_z}(\tilde{p}_1, \tilde{p}_2, \lambda_1, \lambda_2) = R_{\lambda_1 \lambda_2}^{SS_z}(x, k_\perp) \phi(x, k_\perp), \quad (10)$$

where $\phi(x, k_\perp)$ describes the momentum distribution of the constituents in the bound state

$$\phi(x, k_\perp) = \mathcal{N} \sqrt{\frac{dk_z}{dx}} \exp\left(-\frac{\vec{k}^2}{2\omega^2}\right) \quad (11)$$

with ω being the meson scale parameter and $R_{\lambda_1\lambda_2}^{SS_z}$ constructs a state of definite spin (S, S_z) out of light-front helicity (λ_1, λ_2) eigenstates. Explicitly, in practice it is more convenient to use the covariant form for $R_{\lambda_1\lambda_2}^{SS_z}$ [27]:

$$R_{\lambda_1\lambda_2}^{SS_z}(x, k_\perp) = \frac{\sqrt{p_1^+ p_2^+}}{\sqrt{2} \widetilde{M}_0} \bar{u}(p_1, \lambda_1) \Gamma v(p_2, \lambda_2), \quad (12)$$

where

$$\Gamma = \begin{cases} \gamma_5 & (\text{pseudoscalar } S=0) \\ -\not{\epsilon}(S_z) + \frac{\hat{\epsilon} \cdot (p_1 - p_2)}{M_0 + m_1 + m_2} & (\text{vector } S=1) \end{cases} \quad (13)$$

and

$$\widetilde{M}_0 \equiv \sqrt{M_0^2 - (m_1 - m_2)^2} \quad (14)$$

with

$$M_0^2 = \frac{m_1^2 + k_\perp^2}{(1-x)} + \frac{m_2^2 + k_\perp^2}{x} \quad (15)$$

We normalize the meson state as

$$\langle M(P', S', S'_z) | M(P, S, S_z) \rangle = 2(2\pi)^3 P^+ \delta^3(\tilde{P}' - \tilde{P}) \delta_{S'S} \delta_{S'_z S_z}, \quad (16)$$

so that the normalization condition of the momentum distribution function can be obtained

$$\int \frac{dx d^2 k_\perp}{2(2\pi)^3} |\phi(x, k_\perp)|^2 = 1. \quad (17)$$

We note that the form factors in Eq. (4) depend on the meson ($M = q_1 \bar{q}_2$) wave functions $\Psi_M(x, k_\perp)$. To fix the parameters in the wave functions, one may use the meson decay constants f_M , given by

$$f_M = \sqrt{24} \int \frac{dx d^2 k_\perp}{2(2\pi)^3} \Psi_M(x, k_\perp) \frac{\mathcal{A}}{\sqrt{\mathcal{A}^2 + k_\perp^2}}, \quad (18)$$

where $\mathcal{A} = m_{q_1} x + m_{q_2} (1-x)$ with m_{q_i} being the composed quark masses.

In our numerical study, we use $f_{B_s} = 200 \text{ MeV}$, and $f_{\eta_s} = (1.34 \pm 0.06) f_\pi$ [21] which is the decay constant of the constituent bound state $s\bar{s}$. By putting these decay constants into Eq. (18), we get the adapted ω value for the wave function in Eq. (11). Explicitly, we find that $\omega_{B_s} = 0.56$ and $\omega_{\eta_s} = 0.45 \text{ GeV}$.

In Figure 2, we display the form factors as functions of $s = q^2/M_{B_s}^2$ for the transitions of $B_s \rightarrow \eta_s$ (with physical masses $m_{\eta, \eta'}$) and $B_s \rightarrow \phi$ with the parameters in Table 2. In

Table 3, we show the form factors of the pseudoscalar daughter meson with $q^2 = 0$. Since F_+ does not depend on the daughter meson mass, we find that F_+ has the same value for both m_η and $m_{\eta'}$, whereas F_- and F_T are different. The form factors for $B_s \rightarrow \phi$ including vector and tensor current matrix elements are given in Table 4. We note that we have used the same scale parameter for the pseudoscalar and vector mesons. In Tables 3 and 4, we have also listed the results in the CQM [17] as comparisons.

We note that, as shown in Figure 2, there are deviations for the form factors, in particular F_T , between the LFQM and CQM for the region of large q^2 values. As we know that in the LFQM the form factors are calculated in all physical q^2 region, some form factors, such as F_T , could increase as q^2 near the zero recoil point since the matrix elements depend on the overlap integral of the initial and final meson wave functions. While in the CQM [17], all form factors have similar q^2 behaviors since they have the same double pole forms of

$$\frac{F_i(q^2)}{F_i(0)} = \frac{1}{1 + \sigma_1 s + \sigma_2 s^2} \quad (19)$$

where $s = q^2/m_{B_s}^2$, $F_i(0)$ are the form factors at $q^2 = 0$, and $\sigma_{1,2}$ are the fitted parameters.

Table 2: The parameters used in the calculation of the form factors (in GeV).

| m_{B_s} | m_η | $m_{\eta'}$ | m_ϕ | m_b | m_s | f_{B_s} | f_{η_s} | w_{B_s} | w_{η_s} |
|-----------|----------|-------------|----------|-------|-------|-----------|--------------|-----------|--------------|
| 5.3696 | 0.5473 | 0.9578 | 1.0194 | 4.85 | 0.35 | 0.200 | 0.183 | 0.56 | 0.45 |

Table 3: Form factors $F_{\pm,T}$ for $B_s \rightarrow \eta_s(m_\eta, m_{\eta'})$ transitions at $q^2 = 0$ in the LFQM and CQM.

| | $B_s \rightarrow \eta_s(m_\eta)$ | | | $B_s \rightarrow \eta_s(m_{\eta'})$ | | |
|------|----------------------------------|--------|--------|-------------------------------------|--------|--------|
| | F_+ | F_- | F_T | F_+ | F_- | F_T |
| LFQM | 0.354 | -0.360 | -0.369 | 0.354 | -0.324 | -0.404 |
| CQM | 0.357 | -0.304 | -0.365 | 0.357 | -0.304 | -0.390 |

Table 4: Form factors $V, A_{0,\pm}, g$ and $a_{0,+}$ for $B_s \rightarrow \phi$ for $B_s \rightarrow \phi$ transitions at $q^2 = 0$ in the LFQM and CQM.

| | $B_s \rightarrow \phi$ | | | | | | |
|------|------------------------|--------|-------|--------|-------|-------|--------|
| | V | A_0 | A_+ | A_- | g | a_0 | a_+ |
| LFQM | -0.440 | -0.464 | 0.276 | -0.295 | 0.377 | 0.374 | -0.374 |
| CQM | -0.445 | -0.506 | 0.310 | -0.379 | 0.380 | 0.380 | -0.380 |

3 Decay Rates and Asymmetries

3.1 Decay Rates

Using Eqs. (1), (2), and (4), we obtain the decay amplitudes of $B_s \rightarrow (\eta_s, \phi)\ell\bar{\ell}$ as follows:

$$\mathcal{M}(B_s \rightarrow \eta_s \nu \bar{\nu}) = \frac{G_F}{2\sqrt{2}} \frac{\alpha_{em} \lambda_t}{2\pi \sin^2 \theta_W} D(x_t) F_+ P_\mu \bar{\nu} \gamma^\mu (1 - \gamma_5) \nu, \quad (20)$$

$$\begin{aligned} \mathcal{M}(B_s \rightarrow \phi \nu \nu) = & \frac{G_F}{2\sqrt{2}} \frac{\alpha_{em} \lambda_t}{2\pi \sin^2 \theta_W} D(x_t) \left\{ \frac{1}{m_{B_s} + m_\phi} \left[-iV \varepsilon_{\mu\nu\alpha\beta} \epsilon^{*\nu} P^\alpha q^\beta \right. \right. \\ & \left. \left. + A_0 (P \cdot q) \epsilon_\mu^* + A_+ (\epsilon \cdot P) P_\mu \right] \right\} \bar{\nu} \gamma^\mu (1 - \gamma_5) \nu, \end{aligned} \quad (21)$$

$$\begin{aligned} \mathcal{M}(B_s \rightarrow \eta_s \ell^+ \ell^-) = & \frac{G_F \alpha_{em} \lambda_t}{2\sqrt{2}\pi} \left\{ \left[\left(C_8^{eff} F_+ - \frac{2m_b C_7 F_T(q^2)}{m_{B_s} + m_{\eta(\eta')}} \right) P_\mu \right] \bar{\ell} \gamma^\mu \ell \right. \\ & \left. + [C_9 F_+ P_\mu + C_9 F_- q_\mu] \bar{\ell} \gamma^\mu \gamma_5 \ell \right\}, \end{aligned} \quad (22)$$

$$\begin{aligned} \mathcal{M}(B_s \rightarrow \phi \ell^+ \ell^-) = & \frac{G_F \alpha_{em} \lambda_t}{2\sqrt{2}\pi} \frac{2}{m_{B_s}} \\ & \times \left\{ \left[-i G_V \varepsilon_{\mu\nu\alpha\beta} \epsilon^{*\nu} P^\alpha q^\beta + G_A^0 (P \cdot q) \epsilon_\mu^* + G_A^+ (\epsilon^* \cdot P) P_\mu \right] \bar{\ell} \gamma^\mu \ell \right. \\ & \left. + \left[-i F_V \varepsilon_{\mu\nu\alpha\beta} \epsilon^{*\nu} P^\alpha q^\beta + F_A^0 (P \cdot q) \epsilon_\mu^* \right. \right. \\ & \left. \left. + F_A^+ (\epsilon^* \cdot P) P_\mu + F_A^- (\epsilon^* \cdot P) q_\mu \right] \bar{\ell} \gamma^\mu \gamma_5 \ell \right\}, \end{aligned} \quad (23)$$

where the functions $G_V, F_V, G_A^0, F_A^0, G_A^+, F_A^+$, and F_A^- are defined by

$$\begin{aligned} G_V &= \frac{C_8^{eff} V}{2(1 + \sqrt{r_\phi})} - \frac{C_7 \hat{m}_b g}{s}, & F_V &= \frac{C_9 V}{2(1 + \sqrt{r_\phi})}, \\ G_A^0 &= \frac{C_8^{eff} A_0}{2(1 + \sqrt{r_\phi})} - \frac{C_7 \hat{m}_b a_0}{s}, & F_A^0 &= \frac{C_9 A_0}{2(1 + \sqrt{r_\phi})}, \\ G_A^+ &= \frac{C_8^{eff} A_+}{2(1 + \sqrt{r_\phi})} - \frac{C_7 \hat{m}_b a_+}{s}, & F_A^+ &= \frac{C_9 A_+}{2(1 + \sqrt{r_\phi})}, \\ F_A^- &= \frac{C_9 A_-}{2(1 + \sqrt{r_\phi})}, \end{aligned} \quad (24)$$

with $s = q^2/m_{B_s}^2$, $\hat{m}_b = m_b/m_{B_s}$ and $r_\phi = m_\phi^2/m_{B_s}^2$. From Eqs. (1), (2), (6) and (20)-(23), the differential decay rates for $B_s \rightarrow M_s \nu \bar{\nu}$ are found to be

$$\frac{d\Gamma(B_s \rightarrow M_s \nu \bar{\nu})}{ds} = \frac{G_F^2 |\lambda_t|^2 \alpha_{em}^2 |D(x_t)|^2 m_{B_s}^5}{2^8 \pi^5 \sin^4 \theta_W} \varphi_{M_s}^{1/2} \mathcal{F}_{M_s}, \quad (25)$$

where

$$\begin{aligned} \mathcal{F}_\eta &= \sin^2 \theta \times \varphi_\eta |F_+|^2, \\ \mathcal{F}_{\eta'} &= \cos^2 \theta \times \varphi_{\eta'} |F_+|^2, \\ \mathcal{F}_\phi &= 3s \left[(1 - \sqrt{r_\phi})^2 |A_0|^2 + \frac{\varphi_\phi}{(1 + \sqrt{r_\phi})^2} |V|^2 \right] \\ &+ \varphi_\phi \left[\frac{(1 - \sqrt{r_\phi})^2}{4r_\phi} |A_0|^2 - \frac{s}{(1 + \sqrt{r_\phi})^2} |V|^2 + \frac{\varphi_\phi}{4r_\phi (1 + \sqrt{r_\phi})^2} |A_+|^2 \right. \\ &\left. + \frac{(1 - r_\phi - s)(1 - \sqrt{r_\phi})}{2r_\phi (1 + \sqrt{r_\phi})} \text{Re}(A_0 A_+^*) \right]. \end{aligned} \quad (26)$$

For $B_s \rightarrow M_s \ell^+ \ell^-$ ($\ell = e, \mu, \tau$), we get

$$\frac{d\Gamma(B_s \rightarrow M_s \ell^+ \ell^-)}{ds} = \frac{G_F^2 |\lambda_t|^2 m_{B_s}^5 \alpha_{em}^2}{3 \cdot 2^9 \pi^5} \left(1 - \frac{4t}{s}\right)^{\frac{1}{2}} \varphi_{M_s}^{1/2} \left[\left(1 + \frac{2t}{s}\right) \alpha_{M_s} + t \delta_{M_s} \right], \quad (27)$$

where

$$\begin{aligned} t &= m_\ell^2/m_{B_s}^2, \quad r_{M_s} = m_{M_s}^2/m_{B_s}^2, \\ \varphi_{M_s} &= (1 - r_{M_s})^2 - 2s(1 + r_{M_s}) + s^2. \end{aligned} \quad (28)$$

The formulas of α_{M_s} and δ_{M_s} are given by

$$\begin{aligned} \alpha_\eta &= \sin^2 \theta \times \varphi_\eta \left(|C_8^{eff} F_+ - \frac{2C_7 F_T}{1 + \sqrt{r_\eta}}|^2 + |C_9 F_+|^2 \right), \\ \delta_\eta &= \sin^2 \theta \times 6|C_9|^2 \{ [2(1 + r_\eta) - s] |F_+|^2 + 2(1 - r_\eta) \text{Re}(F_+ F_-^*) + s |F_-|^2 \}, \end{aligned} \quad (29)$$

$$\begin{aligned} \alpha_{\eta'} &= \cos^2 \theta \times \varphi_{\eta'} \left(|C_8^{eff} F_+ - \frac{2C_7 F_T}{1 + \sqrt{r_{\eta'}}}|^2 + |C_9 F_+|^2 \right), \\ \delta_{\eta'} &= \cos^2 \theta \times 6|C_9|^2 \{ [2(1 + r_{\eta'}) - s] |F_+|^2 + 2(1 - r_{\eta'}) \text{Re}(F_+ F_-^*) + s |F_-|^2 \}, \end{aligned} \quad (30)$$

$$\begin{aligned} \alpha_\phi &= 4s \left[3(1 - r_\phi)^2 (|G_A^0|^2 + |F_A^0|^2) + 2\varphi_\phi (|G_V|^2 + |F_V|^2) \right] \\ &+ \frac{\varphi_\phi}{r_\phi} \left[(1 - r_\phi)^2 (|G_A^0|^2 + |F_A^0|^2) + \varphi_\phi (|G_A^+|^2 + |F_A^+|^2) \right. \\ &\left. + 2(1 - r_\phi)(1 - r_\phi - s) \text{Re}(G_A^0 G_A^{+*} + F_A^0 F_A^{+*}) \right] \\ \delta_\phi &= -48\varphi_\phi |F_V|^2 - 72(1 - r_\phi)^2 |F_A^0|^2 + \frac{6[2(1 + r_\phi) - s]}{r_\phi} \varphi_\phi |F_A^+|^2 \\ &+ \frac{6s}{r_\phi} \varphi_\phi |F_A^-|^2 + \frac{12(1 - r_\phi)}{r_\phi} \varphi_\phi \text{Re}(F_A^0 F_A^{+*} + F_A^0 F_A^{-*} + F_A^+ F_A^{-*}). \end{aligned} \quad (31)$$

Table 5: Decay branching ratios of $B_s \rightarrow (\eta, \eta', \phi)\nu\bar{\nu}$.

| | LFQM | CQM |
|---|-------|-------|
| $10^6 \text{Br}(B_s \rightarrow \eta\nu\bar{\nu})$ | 2.34 | 2.17 |
| $10^6 \text{Br}(B_s \rightarrow \eta'\nu\bar{\nu})$ | 2.52 | 2.38 |
| $10^6 \text{Br}(B_s \rightarrow \phi\nu\bar{\nu})$ | 12.02 | 11.65 |

 Table 6: Decay branching ratios of $B_s \rightarrow (\eta, \eta', \phi)\ell^+\ell^-$ without including LD effects.

| Decay Mode | without LD | | | | |
|---|------------|------|----------|-----------|------------|
| | LFQM | CQM | Ref. [9] | Ref. [10] | Ref. [11] |
| $10^7 \text{Br}(B_s \rightarrow \eta e^+e^-)$ | 3.43 | 3.13 | - | - | - |
| $10^7 \text{Br}(B_s \rightarrow \eta\mu^+\mu^-)$ | 3.42 | 3.12 | 4.6, 5.2 | - | - |
| $10^7 \text{Br}(B_s \rightarrow \eta\tau^+\tau^-)$ | 0.67 | 0.67 | - | - | - |
| $10^7 \text{Br}(B_s \rightarrow \eta' e^+e^-)$ | 3.64 | 3.42 | - | - | - |
| $10^7 \text{Br}(B_s \rightarrow \eta'\mu^+\mu^-)$ | 3.63 | 3.41 | - | - | - |
| $10^7 \text{Br}(B_s \rightarrow \eta'\tau^+\tau^-)$ | 0.50 | 0.43 | - | - | - |
| $10^6 \text{Br}(B_s \rightarrow \phi e^+e^-)$ | 1.72 | 1.69 | - | - | 2.01, 1.87 |
| $10^6 \text{Br}(B_s \rightarrow \phi\mu^+\mu^-)$ | 1.64 | 1.61 | - | 2.5 | 1.65, 1.25 |
| $10^7 \text{Br}(B_s \rightarrow \phi\tau^+\tau^-)$ | 1.60 | 1.51 | - | - | 1.38, 2.28 |

By using the form factors of the LFQM and CQM in Figure 2 and $|\lambda_t| = |V_{tb}V_{ts}| \simeq 0.041$, from Eqs. (25) and (27), we now can estimate the numerical values for the decay rates. In Figures 3 and 4, we show the differential decay branching ratios as a function of $s = q^2/m_{B_s}^2$ for $B_s \rightarrow M_s \ell \bar{\ell}$ ($\ell = \nu, e, \mu, \tau$) in the two models, respectively. In Tables 5 and 6, we summarize the BRs of $B_s \rightarrow (\eta, \eta', \phi)\ell^+\ell^-$ ($\ell = \nu, e, \mu, \tau$), where LD effects for the charged lepton modes are not included. In Table 6, we also show the results in Refs. [9], [10] and [11]. In the table, the two values under Ref. [9] represent two inputs of the η mixing parameter and those under Ref. [11] are from two kinds of hadronic models.

With the LD effects, we need to introduce some cuts around the resonances of J/ψ and ψ' . Explicitly, we use the same cut as the one in the CDF experiment [12], which leads to three regions given by

$$\begin{aligned}
 I. \quad & 2m_\ell < \sqrt{q^2} < 2.9; \\
 II. \quad & 3.3 < \sqrt{q^2} < 3.6; \\
 III. \quad & 3.8 < \sqrt{q^2} < m_{B_s} - m_{M_s}.
 \end{aligned} \tag{32}$$

In Table 7, we present the decay BRs in terms of the regions shown in Eq. (32). From Table 7, it is interesting to pointed out that the results of $Br(B_s \rightarrow \phi\mu^+\mu^-) = 1.23(1.24) \times$

10^{-6} in the LFQM (CQM) are about two orders of magnitude less than the recent CDF experimental upper limit of 6.7×10^{-5} [12]. We note that with the LD effects, in Refs. [10, 11] the branching ratio of $B_s \rightarrow \phi \mu^+ \mu^-$ is found to be around 1.9 and $(1.91, 1.45) \times 10^{-6}$, respectively. The values for Ref. [11] were derived with a much smaller cut.

Table 7: Decay branching ratios of $B_s \rightarrow (\eta, \eta', \phi) \ell^+ \ell^-$ with LD effects and the cuts.

| | with LD | | | | | | | |
|---|---------|------|------|------|------|------|----------|-------|
| regions | I | | II | | III | | I+II+III | |
| Decay BR | LFQM | CQM | LFQM | CQM | LFQM | CQM | LFQM | CQM |
| $10^7 \text{Br}(B_s \rightarrow \eta e^+ e^-)$ | 1.86 | 1.81 | 0.32 | 0.28 | 0.61 | 0.49 | 2.79 | 2.59 |
| $10^7 \text{Br}(B_s \rightarrow \eta \mu^+ \mu^-)$ | 1.85 | 1.80 | 0.32 | 0.28 | 0.61 | 0.49 | 2.78 | 2.58 |
| $10^8 \text{Br}(B_s \rightarrow \eta \tau^+ \tau^-)$ | — | — | 0.13 | 0.12 | 4.95 | 5.11 | 5.08 | 5.23 |
| $10^7 \text{Br}(B_s \rightarrow \eta' e^+ e^-)$ | 2.46 | 2.42 | 0.34 | 0.30 | 0.27 | 0.22 | 3.07 | 2.94 |
| $10^7 \text{Br}(B_s \rightarrow \eta' \mu^+ \mu^-)$ | 2.44 | 2.40 | 0.35 | 0.31 | 0.27 | 0.22 | 3.05 | 2.92 |
| $10^8 \text{Br}(B_s \rightarrow \eta' \tau^+ \tau^-)$ | — | — | 0.14 | 0.13 | 3.27 | 2.77 | 3.41 | 2.90 |
| $10^7 \text{Br}(B_s \rightarrow \phi e^+ e^-)$ | 8.71 | 9.04 | 1.88 | 1.83 | 2.56 | 2.23 | 13.15 | 13.10 |
| $10^7 \text{Br}(B_s \rightarrow \phi \mu^+ \mu^-)$ | 7.91 | 8.30 | 1.88 | 1.83 | 2.56 | 2.23 | 12.35 | 12.36 |
| $10^8 \text{Br}(B_s \rightarrow \phi \tau^+ \tau^-)$ | — | — | 0.48 | 0.48 | 8.87 | 8.31 | 9.35 | 8.80 |

3.2 Asymmetries

The forward-backward asymmetry (FBA) in the charged lepton decay is defined by

$$\mathcal{A}_{FB} = \frac{\int_0^1 d(\cos \theta_\ell) d\Gamma - \int_{-1}^0 d(\cos \theta_\ell) d\Gamma}{\int_0^1 d(\cos \theta_\ell) d\Gamma + \int_{-1}^0 d(\cos \theta_\ell) d\Gamma} \quad (33)$$

where θ_ℓ is the angle between the lepton ℓ^+ momentum in the dilepton c.m. frame and the B_s meson decay l.b. frame. In the SM, it is easy to show that the FBAs in $B_s \rightarrow (\eta, \eta') \ell^+ \ell^-$ are equal to zero and the FBA in $B_s \rightarrow \phi \ell^+ \ell^-$ is given by

$$\mathcal{A}_{FB} = \frac{12s\varphi_\phi^{\frac{1}{2}} \left(1 - \frac{4t}{s}\right)^{\frac{1}{2}} (1 - r_\phi) \text{Re}(G_V F_A^{0*} + G_A^0 F_V^*)}{\left(1 + \frac{2t}{s}\right) \alpha_\phi + t \delta_\phi}. \quad (34)$$

In Figure 5, we display $\mathcal{A}_{FB}(s)$ in $B_s \rightarrow \phi \ell^+ \ell^-$ ($\ell = \mu, \tau$) as a function of s . As seen from the figure, $\mathcal{A}_{FB}(B_s \rightarrow \phi \mu^+ \mu^-)$ changes sign at $s = s_0 \simeq 0.1$, i.e., $\mathcal{A}_{FB}(s_0) = 0$, where s_0 satisfies the relation

$$s_0 = \frac{C_7}{C_8^{eff}} \hat{m}_b (1 + \sqrt{r_\phi}) \left(\frac{g}{V} + \frac{a_0}{A_0} \right). \quad (35)$$

Similar to $B \rightarrow K^* \ell^+ \ell^-$ with $\ell = e$ or μ , the location of s_0 depends on the WCs and is insensitive to the hadronic uncertainties [5, 28].

By writing the unit vector of $\hat{n} = \frac{\vec{p}_\ell}{|\vec{p}_\ell|} = \pm 1$, we can define the longitudinal lepton polarization asymmetry in $B_s \rightarrow M_s \ell^+ \ell^-$ as follows

$$P_L(s) = \frac{\frac{d\Gamma(\hat{n}=-1)}{ds} - \frac{d\Gamma(\hat{n}=1)}{ds}}{\frac{d\Gamma(\hat{n}=-1)}{ds} + \frac{d\Gamma(\hat{n}=1)}{ds}}. \quad (36)$$

From Eqs. (22), (23) and (36), P_L in $B_s \rightarrow P \ell^+ \ell^-$ ($P = \eta, \eta'$) and $B_s \rightarrow \phi \ell^+ \ell^-$ are given by

$$P_L^P = (C_\theta^P)^2 \times \frac{2 \left(1 - \frac{4t}{s}\right)^{\frac{1}{2}}}{\left(1 + \frac{2t}{s}\right) \alpha_P + t \delta_P} \text{Re} \left[\varphi_P \left(C_8^{eff} F_+ - 2 \frac{C_7 F_T}{1 + \sqrt{r_P}} \right) (C_9 F_+)^* \right] \quad (37)$$

$$P_L^\phi = \frac{2 \left(1 - \frac{4t}{s}\right)^{\frac{1}{2}}}{\left(1 + \frac{2t}{s}\right) \alpha_\phi + t \delta_\phi} \text{Re} \left\{ \frac{1}{r_\phi} \left[\varphi_\phi^2 G_A^+ F_A^{+*} + \varphi_\phi (1 - r_\phi) (1 - r_\phi - s) \right. \right. \\ \left. \left. (G_A^0 F_A^{+*} + G_A^+ F_A^{0*}) + (\varphi_\phi + 12 r_\phi s) (1 - r_\phi)^2 G_A^0 F_A^{0*} + 8 \varphi_\phi r_\phi s G_V F_V^* \right] \right\} \quad (38)$$

respectively, where $C_\theta^\eta = -\sin \theta$ and $C_\theta^{\eta'} = \cos \theta$.

In Figure 6, we show the longitudinal lepton polarizations in $B_s \rightarrow (\eta, \eta', \phi) \ell^+ \ell^-$ with $\ell = \mu$ and τ . The results for the electron modes are similar to the muon ones. We remark that, as shown in the figures, $P_L^{\eta, \eta'}(s)$ are close to -1 for the muon modes except the end points of $q_{min}^2 = 4m_\ell^2$ and $q_{max}^2 = (m_{B_s} - m_M)^2$ in which they are zero and they range from -0.4 to 0 and -0.2 to 0 for the τ ones, while the average ones of $\langle P_L^{\eta(\eta')} \rangle$ without LD effects are -0.97(-0.96) and -0.32(-0.17) for the muon and tau modes, respectively. For $B_s \rightarrow \phi \ell^+ \ell^-$, $P_L^\phi(s_{min}) = 0$ but $P_L^\phi(s_{max}) \neq 0$ since φ_ϕ cannot be factorized out in Eq. (38). We have that $\langle P_L^\phi \rangle_\mu = -0.81$ and $\langle P_L^\phi \rangle_\tau = -0.49$.

4 Conclusions

We have studied the rare B_s decays of $B_s \rightarrow (\eta, \eta', \phi) \nu \bar{\nu}$ and $B_s \rightarrow (\eta, \eta', \phi) \ell^+ \ell^-$ ($\ell = e, \mu, \tau$). In our analysis, we have used the form factors of $B_s \rightarrow (\eta, \eta', \phi)$ transitions calculated in the LFQM and CQM. We have found that $Br(B_s \rightarrow \eta \ell \bar{\ell})$ ($\ell = \nu, e, \mu, \tau$) = (23.4, 3.43, 3.42, 0.67) and (21.7, 3.13, 3.12, 0.67) $\times 10^{-7}$, $Br(B_s \rightarrow \eta' \ell \bar{\ell})$ = (25.2, 3.64, 3.63, 0.50) and (23.8, 3.42, 3.41, 0.43) $\times 10^{-7}$, and $Br(B_s \rightarrow \phi \ell \bar{\ell})$ = (12.02, 1.72, 1.64, 0.16) and (11.65, 1.69, 1.61, 0.15) $\times 10^{-6}$ without LD contributions in the two models, respectively. We have also discussed the longitudinal lepton polarization and forward-backward asymmetries in the charged lepton modes. We have shown that the behaviors of the asymmetries are similar to those in $B \rightarrow K^{(*)} \ell^+ \ell^-$. Clearly, some of the above rare B_s decays and asymmetries can be measured at the BTeV and LHC-B

experiments.

Acknowledgments

This work was supported in part by the National Science Council of the Republic of China under contract numbers NSC-91-2112-M-007-043.

References

- [1] Belle Collaboration, J. Kaneko *et al.*, arXiv:hep-ex/0208029.
- [2] Belle Collaboration, K. Abe *et al.*, Phys. Rev. Lett. **88**, 021801 (2002).
- [3] BABAR Collaboration, B. Aubert *et al.*, Phys. Rev. Lett. **88**, 241801 (2002).
- [4] BABAR Collaboration, B. Aubert *et al.*, arXiv:hep-ex/0207082.
- [5] A. Ali, P. Ball, L.T. Handoko, and G. Hiller, Phys. Rev. **D61**, 074024 (2000); P. Colangelo, F. De Fazio, P. Santorelli, and E. Scrimieri, Phys. Rev. **D53**, 3672 (1996); D. Melikhov, N. Nikitin, and S. Simula, Phys. Rev. **D57**, 6814 (1998).
- [6] C.Q. Geng and C.P. Kao, Phys. Rev. **D57**, 4479 (1998).
- [7] A. Ali, E. Lunghi, C. Greub, and G. Hiller, Phys. Rev. **D66**, 034002 (2002); T.M. Aliev, H. Koru, A. Özpineci, and M. Savci, Phys. Lett. **B400**, 194 (1997); T. M. Aliev, M. Savci, and A. Özpineci, Phys. Rev. **D56**, 4260 (1997); G. Burdman, Phys. Rev. **D52**, 6400 (1995); N. G. Deshpande and J. Trampetic, Phys. Rev. Lett. **60**, 2583 (1988); C. Greub, A. Ioannissian, and D. Wyler, Phys. Lett. **B346**, 149 (1995); J. L. Hewett and J. D. Wells, Phys. Rev. **D55**, 5549 (1997); and references therein.
- [8] C.H. Chen and C.Q. Geng, Phys. Rev. **D63**, 114025 (2001); Phys. Rev. **D64**, 074001 (2001).
- [9] P.Z. Skands, JHEP 0101:008 (2001)[arXiv:hep-ph/0010115].
- [10] A. Deandrea and A.D. Polosa, Phys. Rev. **D64**, 074012 (2001).
- [11] G. Erkol and G. Turan, Eur. Phys. J. C **25**, 575 (2002).
- [12] CDF Collaboration (D. Acosta *et al.*), Phys. Rev. **D65**, 111101(R) (2002).
- [13] J.M. Flynn and C.T. Sachrajda, arXiv:hep-lat/9710057.
- [14] P. Ball and V.M. Braun, Phys. Rev. **D58**, 094016 (1998).
- [15] H.Y. Cheng, C.Y. Cheung, and C.W. Hwang, Phys. Rev. **D55**, 1559 (1997).
- [16] C.Q. Geng, C.W. Hwang, C.C. Lih, and W.M. Zhang, Phys. Rev. **D64**, 114024 (2001).

- [17] D. Melikhov and B. Stech, Phys. Rev. **D62**, 014006 (2000).
- [18] T. Inami and C. S. Lim, Prog. Theor. Phys. **65**, 297 (1981).
- [19] G. Belanger and C.Q. Geng, Phys. Rev. **D43**, 140 (1991).
- [20] G. Buchalla and A.J. Buras, Nucl. Phys. **B400**, 225 (1993).
- [21] Th. Feldmann, P. Kroll, and B. Stech, Phys. Rev. **D58**, 114006 (1998).
- [22] M.V. Terent'ev, Sov. J. Phys. **24**, 106 (1976); V.B. Berestetsky and M.V. Terent'ev, *ibid.* **24**, 547 (1976); **25**, 347 (1977).
- [23] P.L. Chung, F. Coester, and W.N. Polyzou, Phys. Lett. **B205**, 545 (1988).
- [24] W.M. Zhang, Chin. J. Phys. **31**, 717 (1994); Preprint IP-ASTP-19-95 [arXiv:hep-ph/9510428].
- [25] C.Y. Cheung, C.W. Hwang, and W.M. Zhang, Z. Phys. **C75**, 657 (1997); C.Q. Geng, C.C. Lih, and Wei-Min Zhang, Phys. Rev. **D57**, 5697 (1998); N.B. Demchuk, I.L. Grach, I.M. Narodetskii, and S. Simula, Phys. Atom. Nucl. **59**, 2152 (1996); Yad. Fiz. **59**, 2235 (1996); I.L. Grach, I.M. Narodetskii, and S. Simula, Phys. Lett. **B385**, 317 (1996).
- [26] A. Dubin and A. Kaidalov, Yad. Fiz. **56**, 164 (1993); Phys. Atom. Nucl. **56**, 237 (1993)].
- [27] W. Jaus, Phys. Rev. **D41**, 3394 (1990); *ibid.* **D44**, 2851 (1991); Z. Phys. **C54**, 611 (1992).
- [28] G. Burdman, Phys. Rev. **D57**, 4254 (1998).

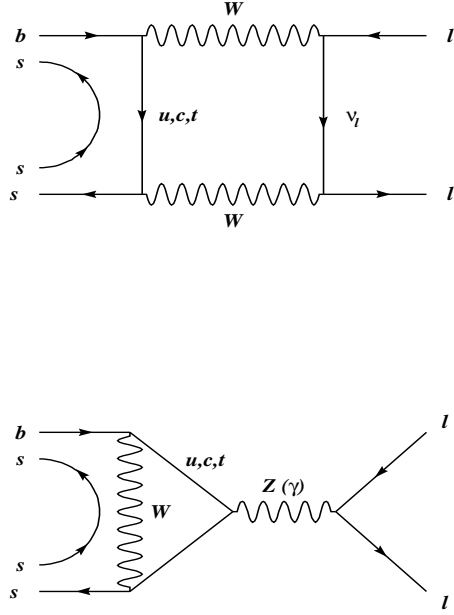


Figure 1: One-loop diagrams for the short-distance contribution in the standard model.

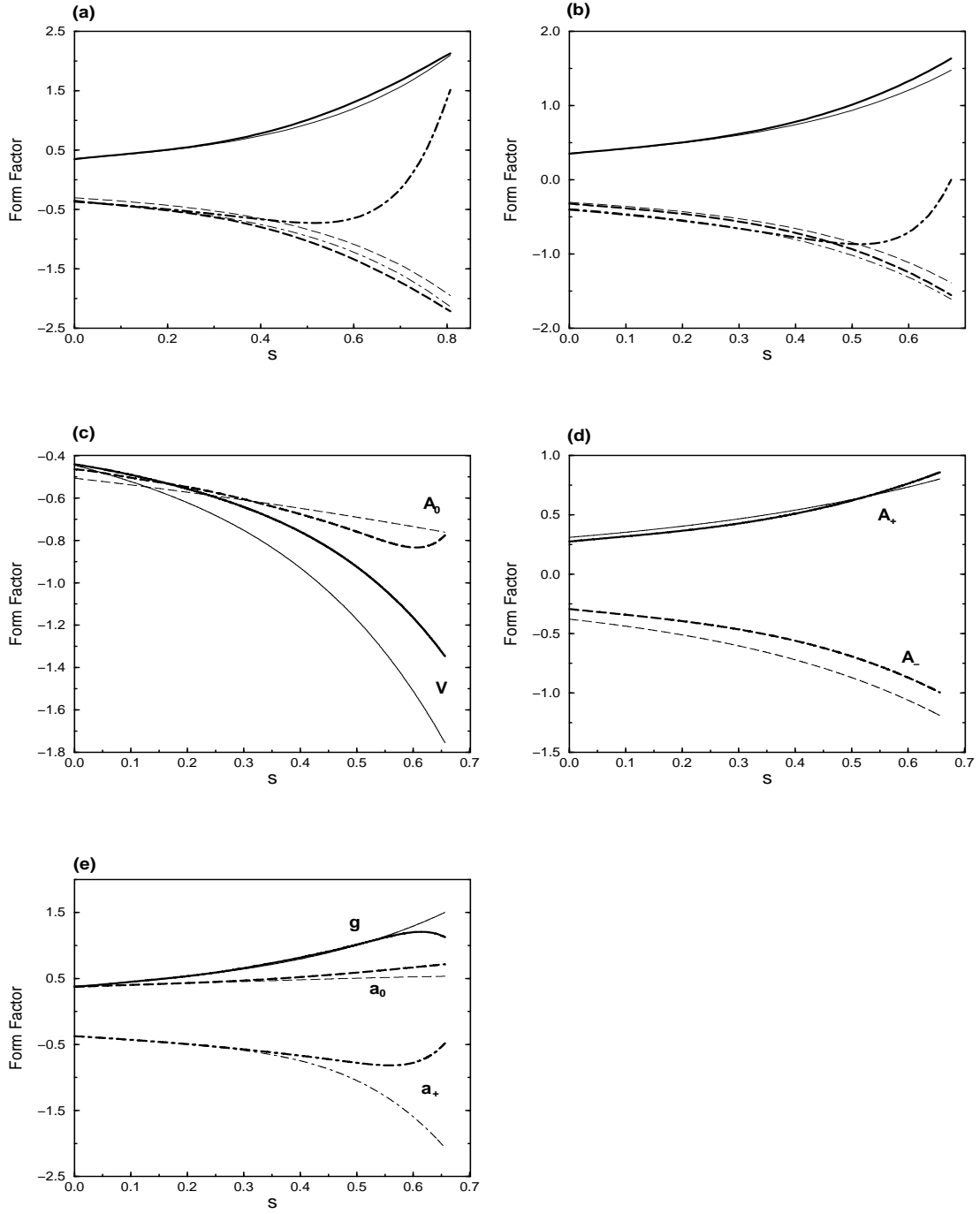


Figure 2: Form factors as functions of $s = q^2/M_{B_s}^2$ for (a) $B_s \rightarrow \eta_s(m_\eta)$ and (b) $B_s \rightarrow \eta_s(m'_\eta)$ with solid, dash, and dash-dot curves representing F_+ , F_- , and F_T , and (c,d,e) $B_s \rightarrow \phi$, respectively. The thick and thin lines stand for the results from the LFQM and CQM, respectively.

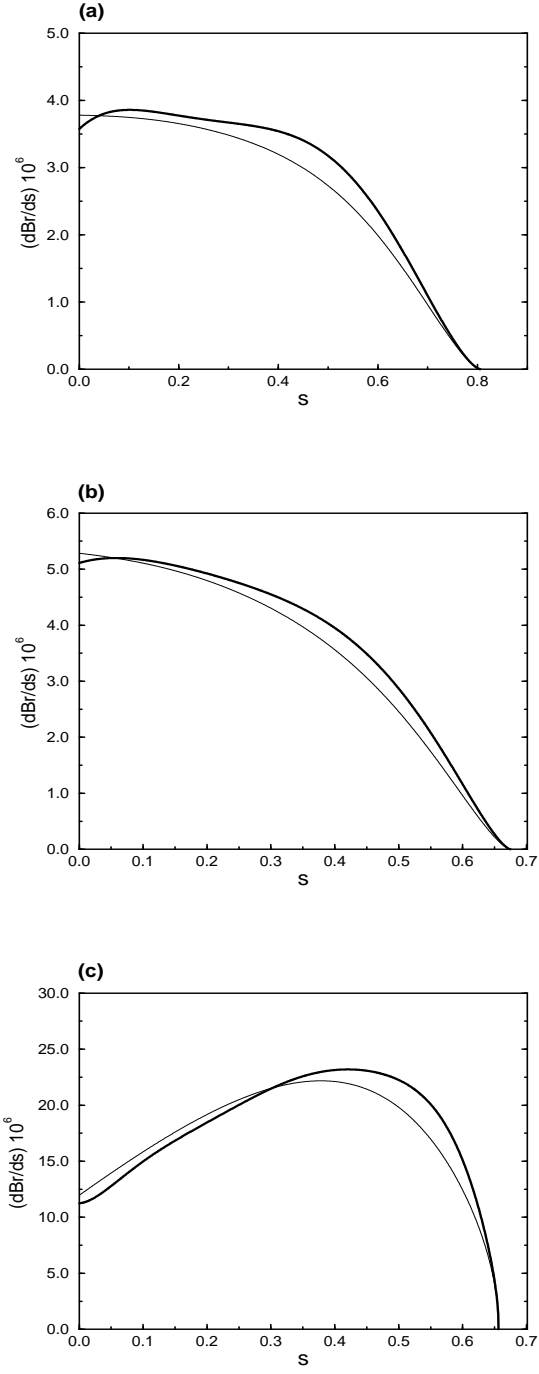


Figure 3: Differential decay branching ratios as a function of $s = q^2/m_{B_s}^2$ for (a) $B_s \rightarrow \eta \nu \bar{\nu}$, (b) $B_s \rightarrow \eta' \nu \bar{\nu}$ and (c) $B_s \rightarrow \phi \nu \bar{\nu}$. Legend is the same as Figure 2.

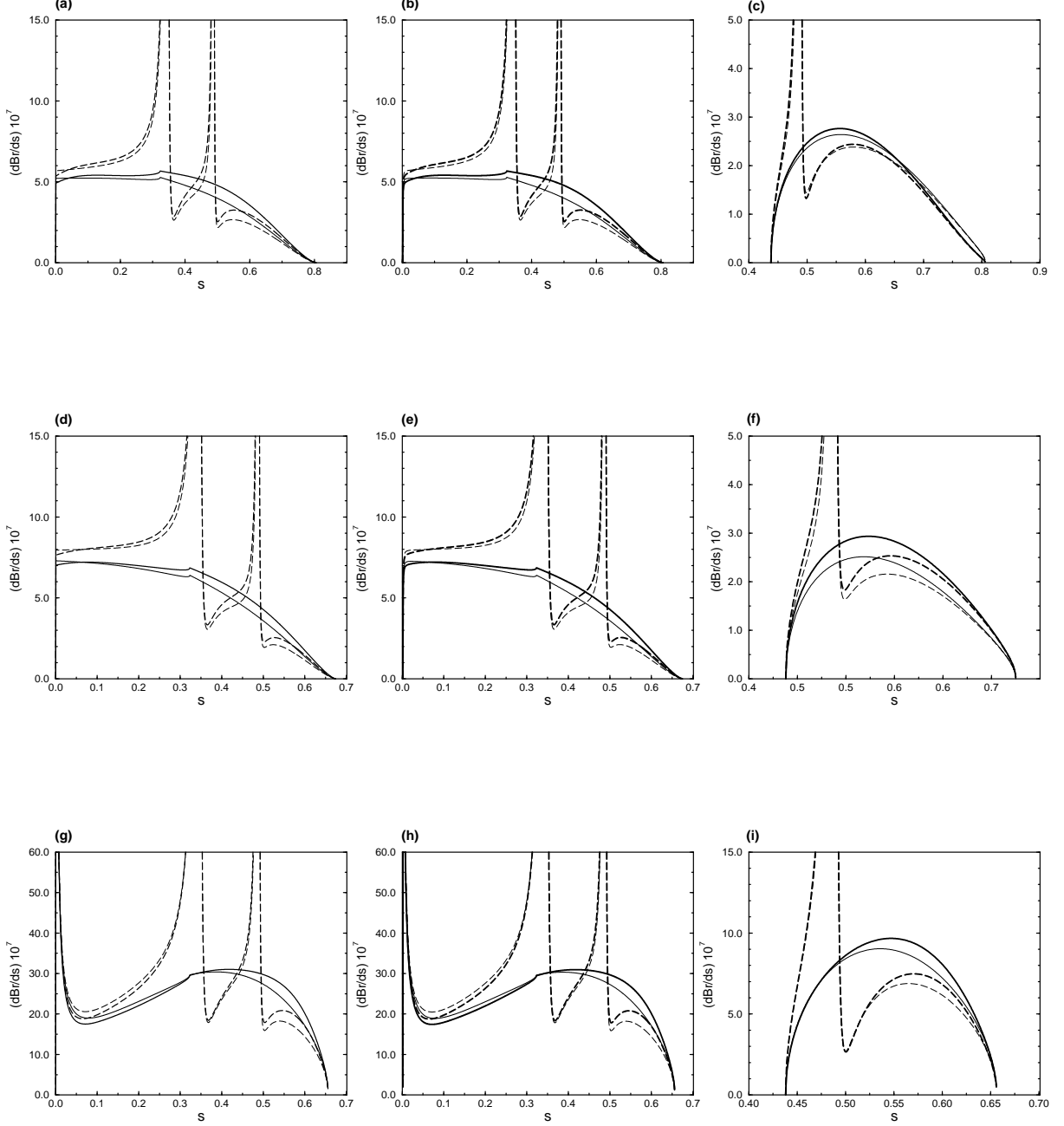


Figure 4: Differential decay branching ratios for $B_s \rightarrow \eta \ell^+ \ell^-$ in (a-c), $B_s \rightarrow \eta' \ell^+ \ell^-$ in (d-f), and $B_s \rightarrow \phi \ell^+ \ell^-$ in (g-i) with $\ell=e, \mu$, and τ , respectively. The curves with (without) resonant shapes represent including (non-including) LD contributions. Legend is the same as Figure 2.

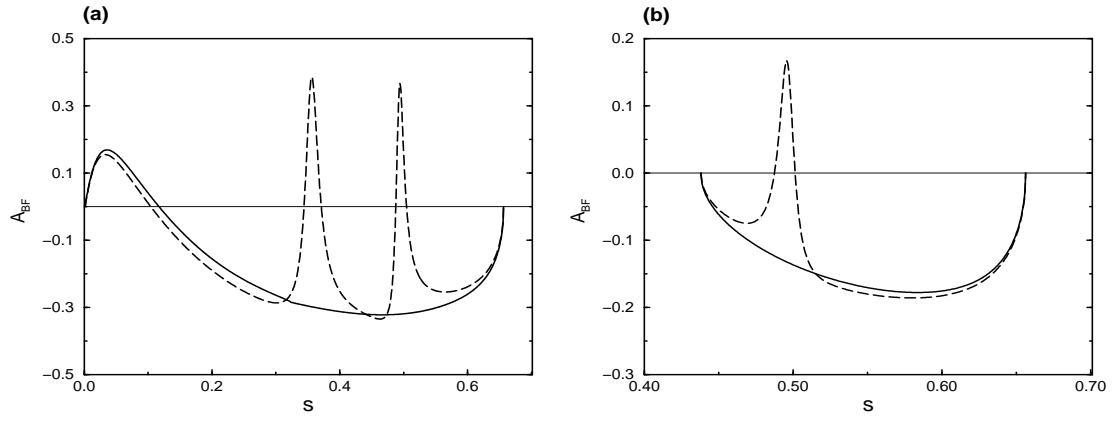


Figure 5: Forward-backward asymmetries in the LFQM for (a) $B_s \rightarrow \phi \mu^+ \mu^-$ and (b) $B_s \rightarrow \phi \tau^+ \tau^-$. Legend is the same as Figure 4.

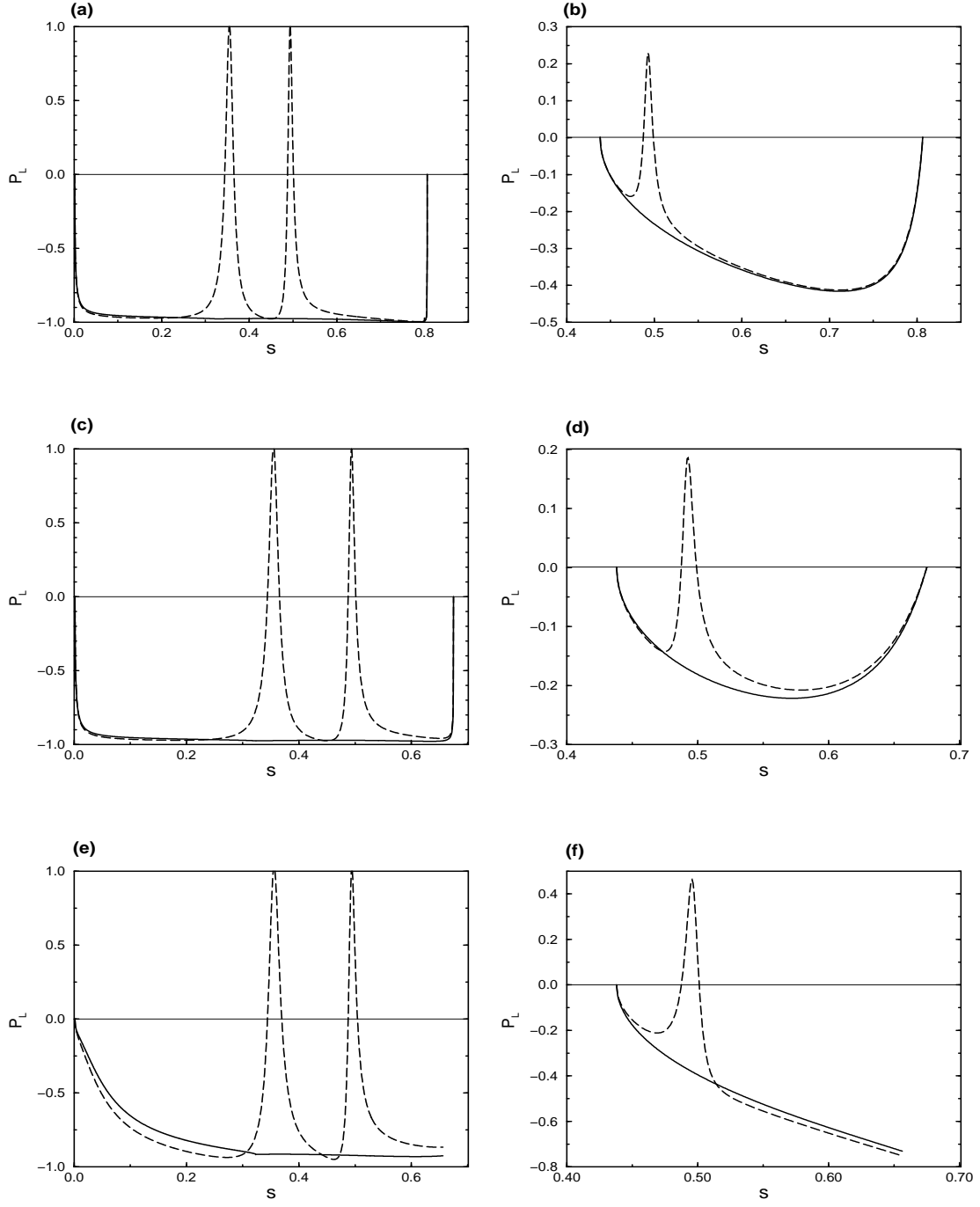


Figure 6: Longitudinal lepton polarization asymmetries in the LFQM for $B_s \rightarrow \eta \ell^+ \ell^-$ in (a,b), $B_s \rightarrow \eta' \ell^+ \ell^-$ in (c,d), and $B_s \rightarrow \phi \ell^+ \ell^-$ in (e,f) with $\ell=(\mu, \tau)$. Legend is the same as Figure 5.